Bioorganic Chemistry 91 (2019) 103137

Contents lists available at ScienceDirect

Bioorganic Chemistry

journal homepage: www.elsevier.com/locate/bioorg

Design, synthesis and biological evaluation of trinary benzocoumarin-thiazoles-azomethines derivatives as effective and selective inhibitors of alkaline phosphatase

Pervaiz Ali Channar[a], Hina Irum[b], Abid Mahmood[b], Ghulam Shabir[a], Sumera Zaib[b], Aamer Saeed[a,*], Zaman Ashraf[c], Fayaz Ali Larik[a], Joanna Lecka[d,e], Jean Sévigny[d,e], Jamshed Iqbal[b,*]

[a] Department of Chemistry, Quaid-i-Azam University, 45320 Islamabad, Pakistan
[b] Centre for Advanced Drug Research, COMSATS University Islamabad, Abbottabad Campus, Abbottabad 22060, Pakistan
[c] Department of Chemistry, Allama Iqbal Open University, Islamabad, Pakistan
[d] Département de microbiologie-infectiologie et d'immunologie, Faculté de Médecine, Université Laval, Québec, QC G1V 0A6, Canada
[e] Centre de Recherche du CHU de Québec – Université Laval, Québec, QC G1V 4G2, Canada

ARTICLE INFO

Keywords:
Coumarin
Thiazole
Azomethine
Tissue-nonspecific alkaline phosphatase
Human intestinal alkaline phosphatase
Anticancer
Design
Synthesis

ABSTRACT

Design, synthesis and characterization of new trinary Benzocoumarin-Thiazoles-Azomethine derivatives having three bioactive scaffolds in a single structural unit were carried out. The newly synthesized molecules were investigated for the inhibitory activity on human tissue nonspecific alkaline phosphatase (*h*-TNAP) and human intestinal alkaline phosphatase (*h*-IAP) isozymes. All the tested compounds exhibited the potent inhibition profile on both isozymes of alkaline phosphatase *i.e., h*-TNAP and *h*-IAP. Molecular docking studies were performed to explore the putative binding mode of interactions of selective inhibitors. Moreover, the synthesized derivatives were evaluated against cervical cancer cell line, HeLa and a few compounds exhibited significant inhibition in the range of 21.0–69.7%. The derivatives can be potential and selective alkaline phosphatase inhibitors for future studies.

1. Introduction

Purinergic signaling plays a crucial role in normal functioning of various physiological processes in the body such as inflammation, pain perception, blood clotting, apoptosis, immune reactions and smooth muscle contraction [1]. Purinergic signaling pathway is comprised of seven ionotropic P2X receptors ($P2X_{1\text{-}7}$), at least eight metabotropic P2Y receptors ($P2Y_{1,2,4,6,11\text{-}14}$) and four adenosine P1 receptors (A_1,A_{2A},A_{2B},A_3). Extracellular nucleotides (ATP, UTP, ADP) and nucleosides (dephosphorylation of ATP generate adenosine) are chemical messengers involved in purinergic signaling pathway [2]. ATP is released into extracellular space in response to physiological condition or pathological stress such as ischemia, hypoglycemia, hypoxia, inflammation, metabolic disorders and cellular damage [3]. ATP (agonist of P2X and P2Y receptors) is rapidly metabolized by surface located ectonucleotidases into various derivatives, thus facilitating the activation of other purinergic receptors. Ectonucleotidases are membrane bounded enzymes which include ecto-nucleoside triphosphate diphosphohydrolases (ENTPDases), ecto-nucleotide pyrophosphatase/phosphodiesterase (ENPPs), alkaline phosphatases (APs) and ecto-5′-nucleotidases (ecto-5′-NT) [3].

Alkaline phosphatases are membrane bound ecto-nucleotidases which are widely distributed from bacteria to mammals. Alkaline phoshatases are dimeric enzymes that catalyze the wide range physiological and non-physiological substrates through dephosphorylation and transphosphorylation reactions [4,5]. The enzymatic activity of alkaline phosphatases (APs) is due to existence of two Zn^{+2} ions and one Mg^{+2} ion within their catalytic site [6]. In human, APs are further sub-divided to two classes; the tissue specific alkaline phosphatases that cover intestinal alkaline phosphatase, placental alkaline phosphatase and germ cell alkaline phosphatase isoenzymes and tissue-nonspecific alkaline phosphatase which is encoded by various genes [7,1]. Currently, tissue-nonspecific and tissue-specific isozymes can be differentiated based on the amino acid sequence and the level of activation or inhibition (Fig. 1). Tissue-nonspecific alkaline phosphatase is found not only in the developing neural tube, but also in kidneys, liver and

* Corresponding authors.
E-mail addresses: asaeed@qau.edu.pk (A. Saeed), drjamshed@cuiatd.edu.pk (J. Iqbal).

https://doi.org/10.1016/j.bioorg.2019.103137
Received 30 March 2019; Received in revised form 6 July 2019; Accepted 19 July 2019
Available online 23 July 2019

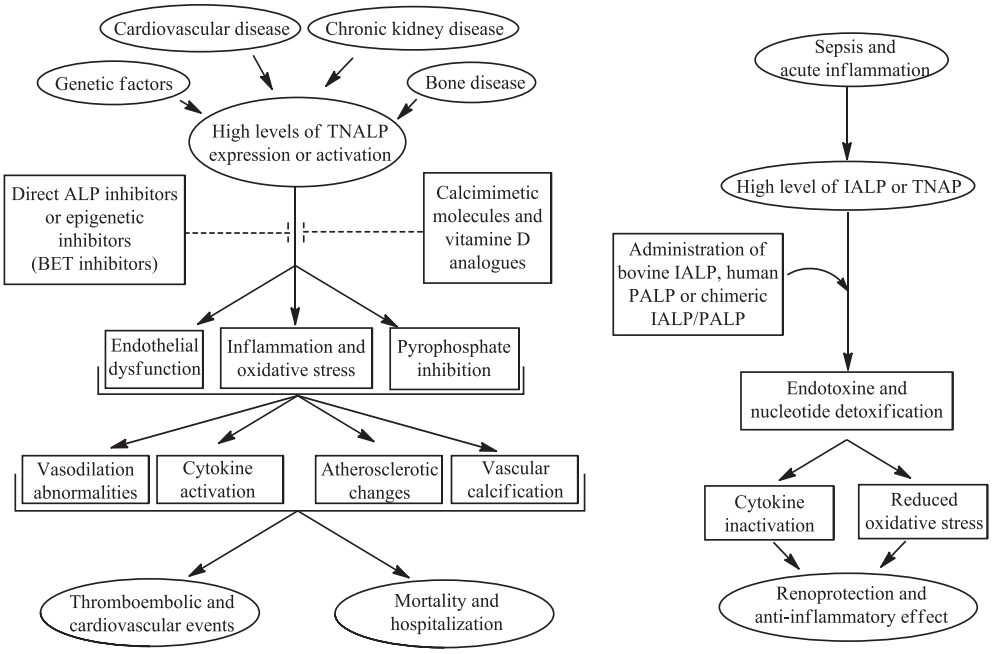

Fig. 1. Pathological indications of increased alkaline phosphatase (ALP) levels [25].

mineralization of tooth and skeletal tissues. The downregulation of TNAP expression can cause rickets/osteomalacia also termed as hypophosphatasia in humans and mice [8]. TNAP is important for the elimination of extracellular inorganic pyrophosphate, which is strong inhibitor of calcification and facilitates normal mineralization of dental and skeletal tissues [9]. Therefore, it is believed that inhibitors of TNAP can be used as drug for the treatment of disease related to pyrophosphate metabolism disorders like various genetic diseases, arterial calcification of infancy and other chronic kidney diseases [10,11]. Previously, different inhibitors have been reported including; levimasole, histidine and homoarginine for TNAP, while L-phenylalanyl-glycyl-glycine (Phe-Gly-Gly) has been reported to inhibit IAP more specifically [7,12]. One of the major drawbacks of known inhibitors is that such inhibitors have been reported to possess various other physiological effects. It remains unclear whether the observed effect is due to inhibition of alkaline phosphatases or by inhibition of any other pathway in which such inhibitors are known to be involved [13].

Therefore, there is a need to design and synthesize selective antagonists for alkaline phosphatases isozymes to well elucidate their specific role. Equally, various nitrogen and sulfur heterocycles with coumarin moieties have recently attracted considerable attention due to the distinctive and unique pharmacological properties including analgesic, antiasthmatic, diuretic, antihypertensive, anticholinergic and anti-inflammatory, etc. [14–17]. Furthermore, the coumarin derivatives comprising thiazole [18], azetidinone [19] and oxazole rings [20] were also found to have antibacterial and antifungal activities. Coumarin derivatives have also been used as intermediates in the processing and production of agrochemicals and pharmaceuticals with significant antibacterial, anticancer and anti-HIV properties [21,22]. Azomethine (containing a –C═N) function) are versatile pharmacophores for design and development of bioactive lead compounds and are found to exhibit anti-inflammatory, analgesic, antimicrobial, anticonvulsant, antitubercular, antimalarial, anticancer, antioxidant, anthelmintic, antiglycation, and antidepressant activities [23,24].

Keeping in view the wide range biological applications of the three individual scaffolds thiazoles, coumarins, and azomethines herein we present a one pot reaction of thiosemicarbazones (**2a-k**) of 3-bromoacetylcoumarin (**1**) in dry ethanol to render a series of compounds (**3a-k**). Conjoining these pharmacophores in a single molecule was targeted to obtain molecules with improved biological properties. The newly synthesized derivatives were screened on the human tissue-nonspecific (*h*-TNAP) and human intestinal alkaline phosphatases (*h*-IAP). Putative binding modes were also investigated inside the active pocket of the homology models of these enzymes and plausible binding interactions were predicted with selective inhibitors.

2. Material and methods

2.1. Apparatus, reagents and chemicals

All commercial reagents were purchased from Sigma-Aldrich. Solvents used were of analytical grade and, when necessary, were purified and dried by the standard methods [26]. Melting points were determined in open capillary tubes on a Stuart melting point apparatus. The FTIR spectra were run on the single beam Nicolet IR 100 (Fourier-Transform). The ^{1}H NMR and ^{13}C NMR spectra were recorded in DMSO-d_6 using NMR Bruker DPX 300 spectrophotometer operating at 300 MHz. TMS was used as internal standard with the deuterium signal of the solvent as the lock and chemical shifts δ recorded in ppm. The elemental analysis (C, H, N, S) of the compounds were performed using Flash EA 1112 elemental analyzer. Compounds were routinely checked by TLC on silica gel G plates using eluting solvents, petroleum ether: ethyl acetate (7: 3, v/v). Also, the developed plates were visualized using a UV lamp for the presence of spots and R_f values were duly calculated.

2.2. Synthesis of 2-(2-(2-Benzylidenehydrazinyl)thiazol-4-yl)-3H-benzo[f] chromen-3-ones

The detailed characterization data along with the synthesis procedures have been provided in supporting information file

2.3. Biochemical assays

2.3.1. Cells transfection for alkaline phosphatases

h-TNAP and *h*-IAP were expressed by plasmid transfection in COS-7 cells [27]. Cells were incubated at 37 °C for the enough time to reach the confluence level of 80–90%. Transfection was performed by

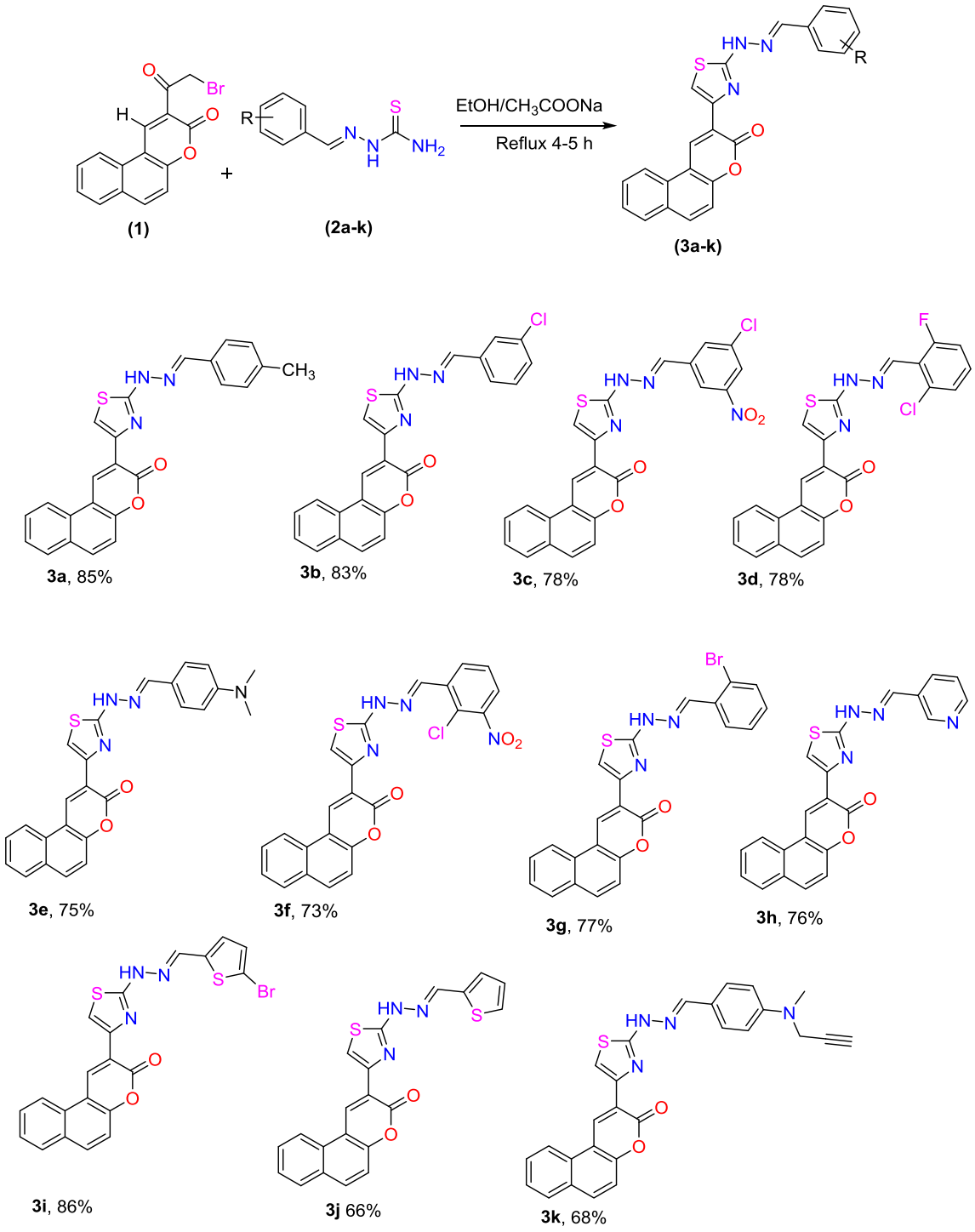

Scheme 1. One pot synthesis of coumarinyl thiazoles (**3a-k**).

transferring the cells to Dulbecco's modified Eagle's medium (DMEM) containing 6 μg of plasmid DNA and 24 μL of lipofactamine reagent. Cells were incubated at 37 °C with 5% CO_2 humidity for 40–72 h and then harvested for the expression analysis [27].

2.3.2. Preparation of membrane fraction

Transfected cells were washed with cold 45 mM Tris-Buffer saline with pH 7.5 containing NaCl (95 mM) phenylmethylsulfonyl fluoride (0.1 mM) and harvested from cell culture plate by scrapping. Cells were washed with same buffer by centrifugation at 300*g* for 5 min at 4 °C and re-suspended in Tris-buffer saline containing 10 μg/mL aprotinin [28]. Protein was quantified by Bradford microplate assay. Supernatant was preserved by adding glycerol (final conc. of 7.5%) and kept at −80 °C [29].

2.3.3. Alkaline phosphatase inhibition assays (h-TNAP and h-IAP):

Inhibitory assay was performed by already mentioned protocol [6,30]. Test compounds were analyzed at 200 μM in DEA buffer. In the first step, 20 μL of *h*-TNAP (47 ng protein/well) or *h*-IAP (56 ng protein/well) treated with 10 μL of test compound. After 5–10 min incubation at 37 °C, 20 μL of CDP-Star® substrate was added. Luminescence was

Table 1
Inhibitory efficacy of coumarinyl thiazoles against human TNAP and IAP.

Codes	*h*-TNAP	*h*-IAP
	IC_{50} ± SEM (μM)	
3a	1.50 ± 0.11	1.32 ± 0.07
3b	2.90 ± 0.14	1.08 ± 0.09
3c	1.81 ± 0.08	1.80 ± 0.12
3d	1.08 ± 0.06	2.28 ± 0.13
3e	1.31 ± 0.10	1.46 ± 0.10
3f	1.04 ± 0.05	2.25 ± 0.13
3g	2.63 ± 0.13	1.36 ± 0.06
3h	0.88 ± 0.03	1.55 ± 0.11
3i	2.08 ± 0.12	1.17 ± 0.10
3j	1.13 ± 0.09	1.02 ± 0.04
3k	0.76 ± 0.02	1.18 ± 0.10
Levamisole	19.2 ± 0.01	–
L-Phenylalanine	–	80.1 ± 0.01

recorded by microplate reader (BioTek FLx800, Instruments, Inc. USA) as after-read. The data was analyzed by PRISM 5.0 (GraphPad, San Diego, California, USA) and IC_{50} values were determined for those test compounds which possessed inhibition more than 50%.

2.4. Molecular docking methodology

2.4.1. Selection of protein structure and preparation of ligands

X-ray crystallographic structures of *h*-TNAP and *h*-IAP are not available in the Protein Data Bank, therefore, for this purpose, already reported homology models from our group were used for docking [30]. The MOE site finder was used for the selections of binding site of the receptor, keeping the catalytic zinc ions in the center of the active site [31]. Preparation of protein structures was carried out by MOE and the structure was protonated by AMBER99 force field. The minimization was done by the RMSD gradient of 0.05 kcal/mol [31]. The compound structures were prepared by MOE builder, and afterwards addition of hydrogen atoms was done by assigning the charges. At the end the energy minimization of compounds structure was carried out by the force field MMFF94x keeping RMSD gradient of 0.01 kcal/mol Å [32].

2.4.2. Docking experiment

The docking analysis of compounds was carried out by LeadIT (BioSolveIT GmbH, Germany) [33]. The docking studies of the selected compounds (selective and dual inhibitors) as well as the reference standards (used in *in vitro* assay), were carried out using default parameters for docking. The top 50 docked poses were selected for each ligand and further analysis was carried out by HYDE assessment [34]. The final pose was selected having lowest binding free energy and the best binding affinity with the receptor and 3D interaction poses were selected using Discovery Studio Visualizer [35].

2.5. Cell viability assays (MTT Assay)

MTT assay was used to determine the antiproliferative potential of test samples (**3a-k**) against HeLa and MCF-7 cell lines after certain modification in reported protocol [36,37]. 90 μL of each cell suspension containing about 2.5×10^4 cell/mL were seeded in 96 well plate and left for overnight in CO_2 incubator at 37 °C. After 24 h of incubation, 10 μL of test compound with final concentration of 100 μM was added in triplicate well format. Cisplatin and culture media were used as positive control (reference comparative standard) and negative control, respectively. Further incubated for about 24 h and added 10 μL of MTT reagent to each well and again incubated for about 4 h at 37 °C. 96 well-plate was observed continuously, until the formazan crystal became visual. Dissolve the crystals by adding 100 μL of solubilizing mixture (50% isopropanol and 10% sodium dodecyl sulfate in 0.1 N HCl) followed by gentle shaking at room temperature for 20–30 min. Concentration of dissolved dye was determined as a function of optical density, measured through microplate reader (FLUOstar Omega Microplate Reader, BMG LABTECH GmbH, Ortenberg, Germany) at 570 nm. Background signals were measured at 690 nm. Results were measured as mean of triplicate wells and percent inhibition was measured for each test sample.

3. Results and discussion

3.1. Synthesis

The series of title compounds (**3a-k**) was synthesized in excellent yields and high purity according to the Scheme 1. Separately prepared thiosemicarbazones (**2a-k**) were reacted with 2-(2-bromoacetyl)-3*H*-benzo[*f*]chromen-3-one (**1**) [37] in dry ethanol in presence of sodium acetate to furnish the title compounds (**3a-k**). The FTIR spectra exhibited absorption bands due to N−H, Ar-H, C=O of lactone, C=N of imine, C=C, C=S and C−O, stretching and bending vibrations at 3370–3399, 2985–3180, 1727–1760, 1625–1650, 1515–1535, 1420–1440, 1275–1290, 1110–1150, 840–865 and 790–825 cm^{-1} respectively. Coumarinyl thiazole **3a** showed N−H group peak at 3370 cm^{-1} and C=C−H stretching vibrations at 3168 cm^{-1}. The peak at 1727 cm^{-1} due to lactonic carbonyl while those of N−H, C=C−H and C=O stretching vibrations are common in all benzocoumarin-thiazoles-azomethines.

The ^{1}H NMR spectrum of compound **3a** showed a 3H singlet peak at 2.32 ppm due to CH_3 group attached to benzene ring. The singlet at 12.25 ppm is due to N−H substituted by heterocyclic and phenyl rings of coumarin. The distinctive peak for all coumarins is the presence of coumarin H-4 at 9.25 ppm. In ^{13}C NMR of **3a** the carbonyl and imine carbons appeared at 169.3 and 159.1 ppm respectively, while the methyl carbon at benzene ring appeared at 21.0 ppm. Similarly, other compounds **3b-k** have been confirmed from their respective ^{1}H NMR and ^{13}C NMR spectra.

3.2. Biological activities

3.2.1. Alkaline phosphatase inhibitory activity

The benzocoumarin-thiazoles-azomethine derivatives were tested for the determination of their inhibitory potential against alkaline phosphatase isozymes *i.e., h*-TNAP and *h*-IAP. The results presented in Table 1 reveal that most of the investigated compounds exhibited selective and potential inhibition towards tissue non-specific alkaline phosphatase. However, few of the compounds were found as selective inhibitors of intestinal alkaline phosphatase.

3.2.2. Structure activity relationship

Among the screened compounds, **3k** and **3h** were noted as the potent inhibitors of ***h*-TNAP** having an inhibitory concentration of 0.76 ± 0.02 and 0.88 ± 0.03 μM, respectively. When the IC_{50} values of these compounds were compared with the inhibitory values of reference standard, levamisole (19.2 ± 0.01 μM), it was observed that these analogues possessed much more potential to inhibit the respective isozyme. The structure activity relationship of these analogues suggested that the presence of halogen atom on the respective structures of the compounds may contribute towards their pronounced activity *i.e.,* bromine atom in **3k** and chlorine atom in **3h**. The other compounds from the same series also showed good inhibitory potential against *h*-TNAP with the IC_{50} values ranging from 1.04 ± 0.05 to 2.90 ± 0.14 μM.

The compounds **3j** and **3b** showed maximum inhibition against ***h*-IAP** with an inhibitory concentration of 1.02 ± 0.04 and 1.08 ± 0.09 μM, respectively. Upon detailed study of the structures of the stated compounds, it was revealed that compound **3j** incorporates only pyridine ring and compound **3b** carries chlorobenzene directly

attached to the basic nuclei. These groups impart non-polar behavior to the basic ring which was expected to be responsible for the maximum activity in case of *h*-IAP enzyme. When the IC_{50} values of these compounds were compared with the inhibitory value of reference standard, L-phenylalanine (80.1 ± 0.01 μM), potency of these compounds was maximum and accountable. Rest of the compounds showed inhibition between 1.17 ± 0.10 and 2.28 ± 0.13 μM. Compound **3c** was found non-selective and dual inhibitor of both isozymes, *h*-TNAP and *h*-IAP with the similar inhibitory values *i.e.,* 1.81 ± 0.08 and 1.80 ± 0.12 μM, respectively**.** This dual effect may be due to the presence of 1-chloro-3-methyl-5-nitrobenzene group directly attached to the basic structure.

It was concluded from the results that the presence of halogen atom (Cl) might be possible cause for the maximum activity against *h*-TNAP and the presence of non-polar group (nitrotoluene) exhibited good activity against *h*-IAP.

3.3. Molecular docking studies

For the investigation of the binding interactions of selective and potent inhibitors inside the models of human TNAP and IAP, the docking studies were performed. Due to unavailability of x-ray structures of both the proteins, the homology models were prepared earlier by our group [30]. As there is no ligand present in the modeled structures, the site finder in MOE software was used and active site was constructed before carrying out docking studies. Furthermore, the validation was done with the positive standards used in the biological assay. The binding interactions of the standards were compared with the potent compounds within the active pockets. Within the active site of these isozymes, the presence of catalytic zinc ions plays important role in their interactions with the compounds. The binding interactions for the standards for both the isozymes were depicted in Figs. 2c, 3c. Results of biological studies suggested that derivative **3h** and **3k** were

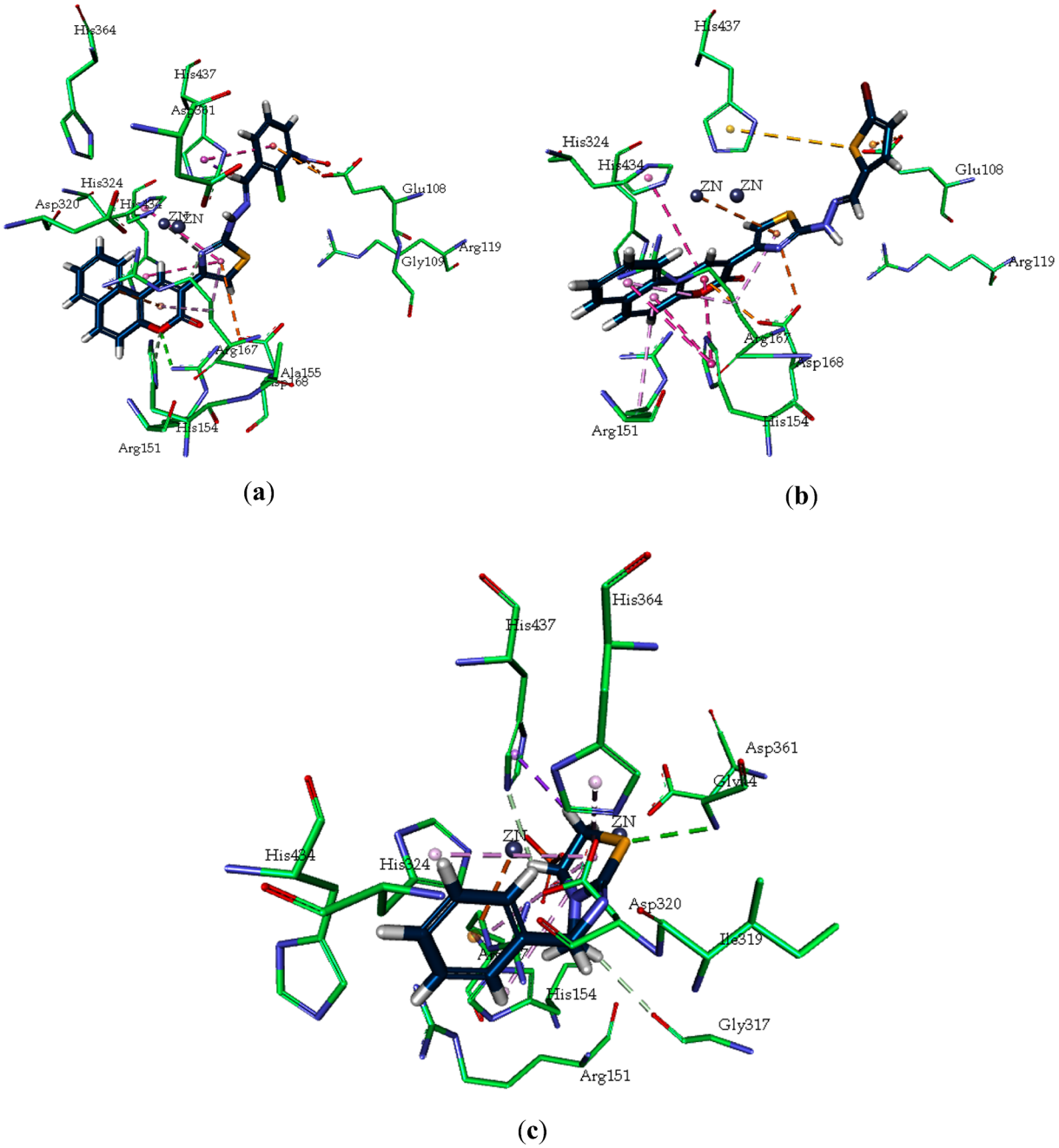

Fig. 2. 3D interactions of compound **3h** (a), **3k** (b) and **Levamisole** (c) within the active site of *h*-TNAP.

potent inhibitor for *h*-TNAP, compound **3b** and **3j** for *h*-IAP. The 3D interaction diagrams for the selected inhibitors were presented in Figs. 2a–b and 3a–b.

3.3.1. Molecular docking studies against human tissue non-specific alkaline phosphatase

Results of biological studies suggested that derivative **3h** and **3k** were potent inhibitor for *h*-TNAP, compound **3b** and **3j** for *h*-IAP. Accordingly, the docking analysis was performed for these selected compounds in their proteins. The binding site interactions of levamisole ((S)-6-phenyl-2,3,5,6-tetrahydroimidazo[2,1-*b*]thiazole) and potent compounds, **3h** and **3k**, in the active pocket of *h*-TNAP unveiled that His364, His437 and His324 were involved in the formation of π-π interactions with the phenyl ring of levamisole and hydrazinylthiazol-4-yl-3*H*-benzo[*f*]chromen-3-one of the compounds. In addition to the π-π interactions, hydrogen bonding was noticed, having profound impact towards the inhibitory profile. The hydrogen bond interactions were observed between basic amino acids and oxygen of the nitrobenzylidene moiety of compound **3h**. Moreover, oxygen of the chrome-3-one of compound **3h** was also found to be involved in hydrogen bonding with Arg167. Similarly, oxygen of the chromen-3-one of compound **3k** was at hydrogen bond distance with Arg167. More residues tangled in the formation of hydrogen bonds were His154, Arg151, Tyr170, His434 and His321. Most important, the metal interactions playing vital role in the inhibition were shown by sulfur of the thiazole moiety of compound **3h** and Zn ion and their bond distance was 4.55 Å. Moreover, the same group of the compound **3k** was involved in the formation of bond with Zn ion and the distance measured was 3.33 Å. However, levamisole was showing interaction with Zn ion having bond distance of 3.72 Å. These kinds of interactions with metals add stability towards the enzyme-inhibitor complex. The 3D interaction diagrams of compound **3h, 3k** and **levamisole** and their binding interactions were depicted in Fig. 2(a, b and c, respectively).

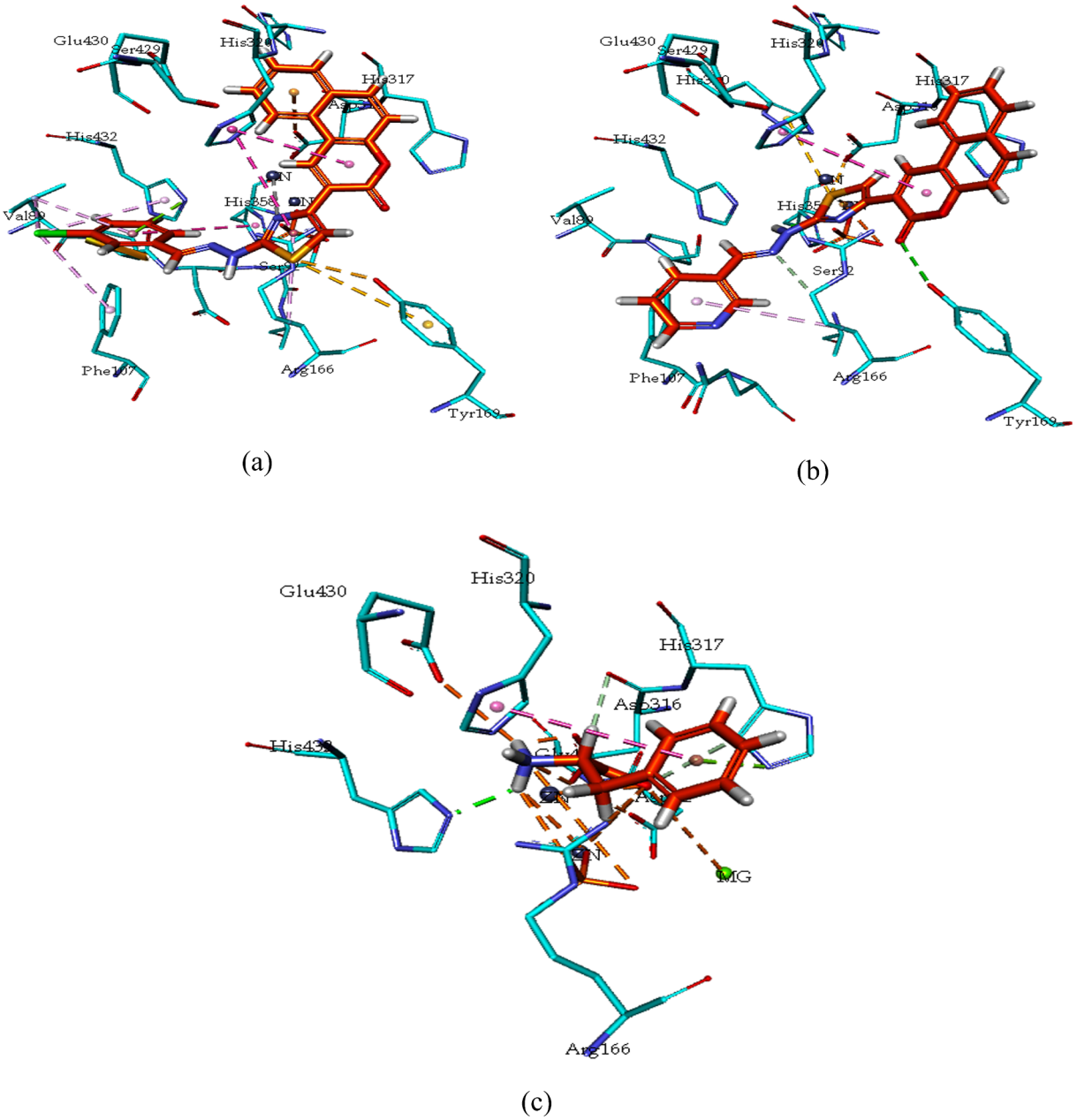

Fig. 3. 3D interactions of compounds **3b** (a), **3j** (b) and **L-phenylalanine** (c) within the active site of *h*-IAP.

3.3.2. Molecular docking studies against human tissue intestinal alkaline phosphatase

Upon investigation of the binding interactions of L-phenylalanine and compound **3b** and **3j** inside the active pocket of *h*-IAP, it came to knowledge that the residues His320, His153, Arg150, His317, Glu108 and Glu321 were mostly involved. The π-π interactions between phenyl part of phenylalanine and His320 were monitored. The similar interactions were also noticed by compound **3b** and His320 and His317 when the 3D diagrams were analyzed. His360 and Arg166 along with Tyr169 were taking part in hydrogen bond formation and the interactions were exhibited in Fig. 3(a, b and c). In *h*-IAP active site, Mg ion was present along with the Zn ions. The ions are taking part in making interactions with L-phenylalanine as well as compound **3j**. The bond distance between thiazole ring and Zn ion in case of compound **3b** was 2.63 Å, however, the bond distance between same group of the compound **3j** and Zn ion was 2.82 Å. The two Zn ions were noted in making interactions with phenylalanine, one with the bond distance of 2.86 Å, however, the second at 4.09 Å. Along with Zinc, magnesium was at bond distance of 5.18 Å from the oxygen of phenylalanine. In addition, the chlorine at the phenyl group of the compound **3b** was directed towards the amino acid Arg150 and His153, and 3*H*-benzo[*f*]chromen-3-one moiety was established in middle of the active site which was well occupied by metal ions. The possible reason for the inhibitory potential may be the orientation of compound **3b** towards the *h*-IAP. The interactions shown by potent compounds, especially the hydrogen bond contributes towards anchoring the selected compounds inside the active pocket of enzyme, thus, providing detailed structural insight of selective compounds in the active site of enzymes.

3.4. In vitro antiproliferative activity against HeLa cervical carcinoma cells and MCF-7 breast cancer cells

The antiproliferative activity of **3a–k** against cervical carcinoma cells (HeLa) and breast cancer cells (MCF-7) was evaluated using MTT [3-(4,5-dimethylthiazol-2-yl)-2,5-diphenyltetrazolium bromide] assay. The percentage inhibition of all the synthetic derivatives was assessed at 100 μM (Table 2). Cisplatin was used as a positive control and exhibited 89.3% growth inhibition at the same concentration level. As cisplatin is known to exhibit highly cytotoxic behavior, most of the derivatives revealed lower antiproliferative activity than cisplatin towards the HeLa cells. All the compounds except **3c, 3f-h** and **3k** exhibited more than 50% inhibition against cancer cells. Compound **3c** (2-(4-(2-(3-chloro-5-nitrobenzylidene)hydrazinyl)thiazol-5-yl)-3*H*-benzo[*f*]chromen-3-one) showed 59.2% inhibition towards HeLa cell lines, compound **3f** (2-(4-(2-(4-chloro-3-nitrobenzylidene)hydrazinyl) thiazol-5-yl)-3*H*-benzo[*f*]chromen-3-one) exhibited 55.8% growth inhibition. However, compound **3g** (2-(4-(2-(2-bromobenzylidene) hydrazinyl)thiazol-5-yl)-3*H*-benzo[*f*]chromen-3-one) have revealed 69.7% inhibition and was the most potent compound after the standard cisplatin. Compound **3h** (2-(4-(2-(pyridin-3-ylmethylene) hydrazinyl) thiazol-5-yl)-3*H*-benzo[*f*]chromen-3-one) have shown 54.6%, while compound **3k** (2-(2-(2-(4-(methyl(prop-2-yn-1-yl)amino)benzylidene) hydrazinyl)thiazol-4-yl)-3*H*-benzo[*f*]chromen-3-one) exhibited 63.1% growth inhibition towards HeLa cell lines. However, the remaining derivatives revealed less inhibition towards HeLa cells. When the cytotoxicity of synthesized derivatives was investigated against breast cancer MCF-7 cell line using MTT assay, it was revealed that none of the compound exhibit cytotoxicity. The results were reported in Table 2. Maximum inhibition found was 28.6% shown by compound **3f**, followed by 24.8% by **3j**, 22.2% by **3h** and 21.6% by compound **3a**. All the other compounds exhibited less %age inhibition and are less toxic to breast cancer cells.

Table 2
Antiproliferative potential of coumarinyl thiazoles **3a-k** against cervical carcinoma cells (HeLa) and breast cancer cells (MCF-7) at 100 μM.

Codes	HeLa	MCF-7
	%age inhibition ± SD	
3a	29.8 ± 2.31	21.6 ± 1.95
3b	36.4 ± 1.17	2.15 ± 1.26
3c	59.2 ± 3.09	1.89 ± 2.07
3d	21.0 ± 0.52	5.13 ± 1.00
3e	42.9 ± 3.26	4.90 ± 1.42
3f	55.8 ± 2.14	28.6 ± 1.20
3g	69.7 ± 1.36	13.2 ± 1.07
3h	54.6 ± 0.98	22.2 ± 1.11
3i	45.3 ± 2.29	18.6 ± 1.89
3j	49.2 ± 3.35	24.8 ± 1.44
3k	63.1 ± 3.14	14.2 ± 1.23
Cisplatin	89.3 ± 1.99	88.9 ± 1.34

4. Conclusions

A series of benzocoumarin-thiazoles-azomethines **3a-k** were synthesized in high yields and investigated against human TNAP and IAP. Most of the derivatives were selective for human TNAP, while some were potential inhibitors of human IAP. 2-(2-(2-(4-(methyl(prop-2-yn-1-yl) amino)benzylidene) hydrazinyl)thiazol-4-yl)-3*H*-benzo[*f*]chromen-3-one, **3k** (IC_{50} = 0.76 ± 0.02 μM) was established to be the most active *h*-TNAP inhibitor, while 2-(4-(2-(thiophen-2-ylmethylene) hydrazinyl) thiazol-5-yl)-3*H*-benzo[*f*]chromen-3-one, **3j** (IC_{50} = 1.02 ± 0.04 μM) was emerged as the potential inhibitor of *h*-IAP. The binding interactions were noteworthy when compared with the interactions shown by reference standards within the active site of human TNAP and IAP. The compounds were screened for their antiproliferative activity on cancer cells (HeLa) and exhibited more than 50% inhibition by compounds **3c, 3f-h** and **3k**. However, the derivatives were not cytotoxic towards breast cancer cell (MCF-7) and all the compounds showed less than 50% inhibition. The results revealed that newly synthesized scaffold may be the interesting molecules and drug targets for future studies. However, it can be recommended that selective inhibitors of *h*-TNAP and *h*-IAP may be chosen further for detailed analysis to explore their inhibitory effects.

Acknowledgements

J.I. is thankful to the Higher Education Commission of Pakistan for the financial support through Project No. Ph-V-MG-3/Peridot/R&D/HEC/2019 and 6927/NRPU/R&D/17. J.S. received support from the Natural Sciences and Engineering Research Council of Canada (NSERC; RGPIN-2016-05867) and was the recipient of a “Chercheur National” Scholarship from the Fonds de Recherche du Québec – Santé (FRQS).

Declaration of Competing Interest

The authors confirm that they have no competing interests.

Appendix A. Supplementary material

Supplementary data to this article can be found online at https://doi.org/10.1016/j.bioorg.2019.103137.

References

[1] M. Al-Rashida, J. Iqbal, Med. Res. Rev. 34 (2014) 703.
[2] F. Di Virgilio, E. Adinolfi, Oncogene 36 (2017) 293.
[3] S. Deaglio, S.C. Robson, Adv. Pharmacol. 61 (2011) 301.
[4] J.L. Millán, Puriner. Signal. 2 (2006) 335.
[5] J.P. Lallès, Nutr. Rev. 72 (2014) 82.
[6] E.A. Sergienko, J.L. Millán, Nat. Protoc. 5 (2010) 1431.
[7] K.A. Lomashvili, P. Garg, S. Narisawa, J.L. Millan, W.C. O’Neill, Kidney Int. 73 (2008) 1024.
[8] S. Narisawa, D. Harmey, M.C. Yadav, W.C. O’Neill, M.F. Hoylaerts, J.L. Millán, J. Bone. Miner. Res. 22 (2007) 1700.
[9] J.L. Millan, Mammalian Alkaline Phosphatases: From Biology to Applications in

Medicine and Biotechnology, Wiley-VCH, Weinheim, Germany, 2006.
[10] S. Sidique, R. Ardecky, Y. Su, S. Narisawa, B. Brown, J.L. Millán, E. Sergienko, N.D. Cosford, Bioorg. Med. Chem. Lett. 19 (2009) 222.
[11] W.H. Fishman, N.K. Ghosh, N.R. Inglis, S. Green, Enzymologia 34 (1968) 317.
[12] H. Bentala, W.R. Verweij, A. Huizinga-Van der Vlag, A.M. van Loenen-Weemaes, D.K. Meijer, K. Poelstra, Shock 18 (2002) 561.
[13] F.S. de Medina, O. Martínez-Augustin, R. González, I. Ballester, A. Nieto, J. Gálvez, A. Zarzuelo, Biochem. Pharmacol. 68 (2004) 2317.
[14] J.A. Hasanen, Der Pharma Chem. 2012 (1923) 5.
[15] L.M. Bedoya, M. Beltrán, R. Sancho, D.A. Olmedo, S. Sánchez-Palomino, E. del Olmo, J.L. López-Pérez, E. Muñoz, A. San Feliciano, J. Alcamí, Bioorg. Med. Chem. Lett. 15 (2005) 4447.
[16] N. Marquez, R. Sancho, L.M. Bedoya, J. Alcamí, J.L. López-Pérez, A. San Feliciano, B.L. Fiebich, E. Muñoz, Antiviral Res. 66 (2005) 137.
[17] F. Bailly, C. Queffelec, G. Mbemba, J.F. Mouscadet, P. Cotelle, Bioorg. Med. Chem. Lett. 15 (2005) 5053.
[18] P.P. Hankare, Jagtap, P.S. Battase, S.R. Naravane, Indian J. Chem. Soc. 79 (2002) 440.
[19] N. Guru, S.D. Srivastava, J. Sci. Ind. Res. 60 (2001) 601.
[20] R.C. Tandel, D. Mammen, Indian J. Chem. 47 (2008) 932.
[21] M.E. Marshall, K. Kervin, C. Benefield, A. Umerani, S. Albainy-Jenei, Q. Zhao, M.B. Khazaeli, J. Cancer Res. Clin. Oncol. 120 (1994) S3.
[22] T. Tanaka, T. Kumamoto, T. Ishikawa, Tetrahedr. Lett. 41 (2000) 10229.
[23] A. Kajal, S. Bala, S. Kamboj, N. Sharma, V. Saini, J. Catal., vol. 2013, Article ID 893512, 14 pages.
[24] M.M. El-Ajaily, A. Maihub, To Chem. J. 1 (1) (2018) 19–37.
[25] M. Haarhaus, V. Brandenburg, K. Kalantar-Zadeh, P. Stenvinkel, P. Magnusson, Nat. Rev. Nephrol. 13 (2017) 429.
[26] Johannes Francois Coetzee (Ed.), Recommended Methods for Purification of Solvents and Tests for Impurities: Inter. Union Pure Appl. Chem. Elsevier, 2013.
[27] Y. Bravo, P. Teriete, R.P. Dhanya, R. Dahl, P.S. Lee, T. Kiffer-Moreira, S.R. Ganji, E. Sergienko, L.H. Smith, C. Farquharson, J.L. Millán, N.D. Cosford, Bioorg. Med. Chem. Lett. 24 (2014) 4308.
[28] F. Kukulski, S.A. Lévesque, E.G. Lavoie, J. Lecka, F. Bigonnesse, A.F. Knowles, S.C. Robson, T.L. Kirley, J. Sévigny, Purinerg. Signal. 1 (2005) 193.
[29] M.M. Bradford, Anal. Biochem. 72 (1976) 248.
[30] I. Khan, A. Ibrar, S.A. Ejaz, S.U. Khan, S.J.A. Shah, S. Hameed, J. Simpson, J. Lecka, J. Sévigny, J. Iqbal, RSC Adv. 5 (2015) 90806.
[31] MOE (Molecular Operating Environment) Version 2016.01. Chemical Computing Group, (CCG). http://www.chemcomp.com/MOEMolecular_Operating_Environment.htm.
[32] P. Labute, Protonate 3D: Assignment of Macromolecular Protonation State and Geometry, Chemical Computing Group, 2007. http://www.chemcomp.com/journal/proton.htm.
[33] LeadIT version 2.3.2; BioSolveIT GmbH, Sankt Augustin, Germany, 2017. www.biosolveit.de/LeadIT.
[34] N. Schneider, G. Lange, S. Hindle, R. Klein, M. Rarey, J. Comput. Aided Mol. Des. 27 (2013) 15.
[35] Dassault Systèmes BIOVIA, Discovery Studio Modeling Environment, Release 2017, DassaultSystèmes, San Diego, 2016.
[36] T. Mosmann, J. Immunol. Meth. 65 (1983) 55.
[37] M. Niks, M. Otto, J. Immunol. Meth. 130 (1990) 149.